Available online at website: https://journal.bcrec.id/index.php/bcrec

Bulletin of Chemical Reaction Engineering & Catalysis, 20 (1) 2025, 166-176

Research Article

Effect of the Dimethylformamide/Isopropanol Solvent Ratio on the Structure, Optical Properties, and Photodegradation Performance of RhB Using Bi-MOF

Pham Bui Bao Long[1], Van Cuong Nguyen[1], Hoang Ai Le Pham[1], Qui Thanh Hoai Ta[2*], Huu Phuc Dang[3*]

[1]Faculty of Chemical Engineering, Industrial University of Ho Chi Minh City, Ho Chi Minh City 700000, Viet Nam.
[2]Institute of Chemical Technology, Vietnam Academy of Science and Technology, 1A TL29 Street, Thanh Loc Ward, District 12, Ho Chi Minh City 70000, Viet Nam
[3]Faculty of Fundamental Science, Industrial University of Ho Chi Minh City, Ho Chi Minh City 70000, Viet Nam.

Received: 27th January 2025; Revised: 20th February 2025; Accepted: 21th February 2025
Available online: 25th February 2025; Published regularly: April 2025

Abstract

This study investigated the structural characteristics, surface morphology, and photocatalytic activity of bismuth-based metal-organic frameworks (BiBTC-ISOx) synthesized with varying ratios of N, N-dimethylformamide (DMF) and isopropanol (ISO). X-ray diffraction confirmed the crystalline structure of the BiBTC-ISOx (x = 1, 3, 6) compounds, while FTIR spectroscopy verified the successful bonding between the ligand and the Bi^{3+} complex. UV-Vis spectroscopy revealed strong UV light absorption with tunable bandgaps ranging from 3.28 to 3.68 eV. Nitrogen adsorption/desorption analysis revealed a hierarchical micro/mesoporous structure, with BiBTC-ISO6 exhibiting the highest surface area (24.968 m^2/g). SEM imaging revealed a rectangular rod-like morphology, which became more elongated with increasing ISO content. The photocatalytic activity of BiBTC-ISOx was evaluated based on the degradation of Rhodamine B (RhB) under visible light, with BiBTC-ISO6 demonstrating the highest efficiency. Optimal conditions for RhB degradation were determined to be 0.03 g catalyst mass, 10 ppm RhB concentration, and pH of 3. Mechanistic studies revealed that superoxide radicals are the primary active species in the photocatalytic process. The BiBTC-ISO6 catalyst exhibited excellent stability and reusability over three consecutive degradation cycles, highlighting its potential for practical applications in organic dye removal.

Keywords: Bi-MOFs; photodegradation; solvent; isopropanol; rhodamine B

How to Cite: Bui Bao Long, P., Nguyen, V. C., Pham, H. A. L., Ta, Q. T. H., Dang, H. P. (2025). Effect of the Dimethylformamide/Isopropanol Solvent Ratio on the Structure, Optical Properties, and Photodegradation Performance of RhB Using Bi-MOF. *Bulletin of Chemical Reaction Engineering & Catalysis*, 20 (1), 166-176. (doi: 10.9767/bcrec.20345)

Permalink/DOI: https://doi.org/10.9767/bcrec.20345

1. Introduction

Water pollution caused by persistent organic contaminants, such as dyes, has become a pressing environmental issue that requires innovative solutions for effective treatment [1,2]. Among these contaminants, Rhodamine B (RhB) stands out because of its widespread use in various industries, including textiles, food, and cosmetics [3–5]. The complex molecular structure and chemical stability of RhB render it resistant to conventional water treatment methods, necessitating the development of advanced degradation strategies. Photocatalysis has emerged as a promising and sustainable approach that leverages light energy to drive the degradation of pollutants into environmentally benign substances [6–9]. The elimination of rhodamine B dye was studied using various

* Corresponding Author.
Email: tathanhhoaiqui2292@ict.vast.vn (Q.T.H. Ta)
danghuuphuc@iuh.edu.vn (H.P. Dang)

techniques, including photocatalytic degradation, adsorption, sedimentation, chemical flocculation, and coagulation. Among these methods, photocatalytic oxidation is recognized as a promising technology for the degradation of organic pollutants. Photocatalysts, which facilitate this process, include solid materials such as titanium dioxide, zinc oxide, metal-doped zinc oxide, graphite carbon nitride, nano metallic materials, and metal-organic frameworks [10–13].

Metal-organic frameworks (MOFs), a class of crystalline porous materials composed of metal nodes and organic linkers, have garnered significant interest in photocatalysis owing to their unique features [14–17]. These include high surface area, tunable porosity, structural diversity, and the ability to incorporate photoactive metal centers. Among various MOFs, bismuth-based MOFs (Bi-MOFs) have shown remarkable potential for photocatalytic applications [18–20]. The favorable electronic properties of bismuth, such as its narrow bandgap and strong visible-light absorption, make it a suitable candidate for photocatalytic degradation of organic pollutants.

Numerous studies have explored the photocatalytic activity of Bi-MOFs in the degradation of organic pollutants [21–23]. For instance, Shanghai Dong *et al*. synthesized a bismuth-based MOF (Bi-BDC) and demonstrated its effectiveness in degrading RhB under visible-light irradiation, attributing its performance to enhanced charge separation and extended light absorption [24]. Similarly, Ya Gao *et al*. developed a Bi-MOF with a hierarchical structure, exhibiting superior photocatalytic efficiency due to its high surface area and robust stability [25]. Another notable study by Zhang *et al*. investigated the photocatalytic degradation of tetracycline using BiBDC with functionalized linkers, highlighting the critical role of linker design in optimizing photocatalytic performance [26]. These studies underline the versatility of Bi-MOFs as photocatalysts and emphasize the importance of material synthesis conditions in determining their properties and performance. Despite these advancements, the influence of synthesis parameters, particularly the solvent system, on the structural, optical, and photocatalytic properties of Bi-MOFs remains underexplored. Solvents play a crucial role in the self-assembly of MOFs by influencing crystal growth, phase purity, and morphology [27]. The influence of solvents on the morphology and photocatalytic properties was previously investigated in $Cu_3(BTC)_2$, zinc-based metal-organic frameworks, and zeolitic imidazolate framework-8 (ZIF-8) [28–30]. In particular, the ratio of the solvents used during synthesis can significantly affect the final properties of MOFs. For example, the mixed-solvent approach involving N,N-dimethylformamide (DMF), and isopropanol (ISO) has been widely used in MOF synthesis to modulate crystallinity and porosity. Understanding how the DMF/ISO ratio affects the structural, optical, and photocatalytic properties of Bi-MOFs can provide valuable insights for tailoring their performances for specific applications.

In this study, we investigated the influence of the DMF/ISO solvent ratio on the structural, optical, and photocatalytic properties of bismuth-based MOF synthesized for RhB degradation. This study systematically examined the effects of varying the solvent ratio on the crystal structure, surface morphology, optical bandgap, and photocatalytic activity under visible-light irradiation. By correlating these properties with the DMF/ISO ratio, this study aims to elucidate the underlying mechanisms that govern the performance of Bi-MOFs in photocatalytic applications.

2. Materials and Methods

2.1 Materials

Bismuth nitrate pentahydrate ($Bi(NO_3)_2.5H_2O$, ≥98%), rhodamin B ($C_{28}H_{31}ClN_2O_3$) (Mw = 626,55 g/mol, λ_{max} = 592 nm) and trimesic acid ($C_9H_6O_6$, benzene-1,3,5-tricarboxylic acid, ≥95%) were purchased from Sigma-Aldrich. The methanol (CH_3OH, ≥98%), N, N-dimethylformamide (C_3H_7NO, ≥99%), isopropanol (C_3H_8O, ≥99.5%), p-benzoquinone ($C_6H_4O_2$, ≥98%), sodium oxalate ($Na_2C_2O_4$, ≥ 99%), potassium dichromate ($K_2Cr_2O_7$, ≥ 98%), nitric acid (HNO_3, 36.5%), hydrochloric acid (HCl, 37%) and sodium hydroxide (NaOH, 98%) were obtained from Xilong Scientific Co., Ltd. All chemicals were used as received. Double-distilled water was used to prepare all solutions.

2.2 Preparation of BiBTC-ISO

0.15 g of $Bi(NO)_3.5H_2O$ (0.303 mmol), and 0.75 g $C_9H_6O_6$ (H_3BTC, 3.4 mmol) (the molar ratio of $Bi(NO)_3.5H_2O$ and H_3BTC is 1:10) were dissolved in 60 mL of N, N-dimethylformamide (DMF) and isopropanol (ISO) at ratios of 5:1, 3:3, and 0:6 (v/v) and stirred for 30 min. The resulting mixture was then transferred to a Teflon container and heated at 120 °C for 24 h. Subsequently, the product was filtered and centrifuged at 6000 rpm for 10 min, washed three times with DMF (20-25 mL, three times), and centrifuged for 10 min. The solid was washed twice with methanol (20-25 mL per wash). The final opaque white BiBTC product was obtained by drying the solid under vacuum at 80 °C for 24 h. The samples are designated as BiBTC-ISOx (x = 1, 3, 6 relate to DMF/ISO ratio (5:1, 3:3, 0:6)).

2.5 Characterizations

X-ray diffraction (XRD) analysis was performed using a LabX XRD-6100 (Shimadzu, Japan) with Cu-Kα radiation, scanning over a 2θ range of 5° to 75° in incremental steps. Fourier transform infrared (FTIR) spectra were obtained using a Bruker Tensor 27 spectrophotometer (4000–400 cm^{-1}) using pressed KBr pellets. The surface morphologies and elemental distributions of the BiBTC-ISO samples were examined using a HR-TEM (TESCAN MIRA). UV–Vis diffuse reflectance spectroscopy (UV–Vis DRS) was conducted using an Agilent Cary 4000 spectrophotometer. UV–Vis spectra of the RhB solutions were obtained using an Agilent Cary 3500 spectrophotometer. Bernauer-Emmett-Teller (BET) measurements using Microtrac's BELSORP MR1. Photocurrent and electrochemical impedance spectroscopy (EIS) measurements were performed using a CHI 660D instrument.

2.6 Photodegradation activity

A 250 mL dual-layer alternating glass beaker was used for the photocatalytic degradation of RhB. A mixture of 0.05 g catalyst and 50 mL RhB (50 mg/L) was stirred in the dark for 60 min to reach equilibrium, with tests conducted at pH 7. Visible light from Xlamp LEDs (4 × 10 W) initiated the photocatalytic process at room temperature. After decomposition, 4 mL of the mixture was sampled at intervals, centrifuged at 30 rpm to remove the catalyst particles, and analyzed using UV-Vis spectrophotometry. The RhB degradation rate was calculated using the Equation (1):

$$H\% = (1 - \frac{C_t}{C_0}) \times 100 \quad (1)$$

C_0 and C_t are the initial concentration of RhB and after irradiation t min, respectively.

3. Results and Discussion

3.1 Preparation, Structural Characterization and Surface Morphology

Previous studies predominantly utilized dimethylformamide (DMF) as the primary solvent in MOF synthesis. However, since DMF is a toxic solvent and our goal is to develop environmentally friendly materials, we introduced isopropyl alcohol to mitigate its toxicity. DMF is a highly potent solvent capable of effectively dissolving polar compounds, including metals and organic acids such as H_3BTC (benzene-1,3,5-tricarboxylic acid). It provides a favorable environment for MOF formation by facilitating the coordination between metal ions and organic linkers. In contrast, isopropyl alcohol, a less polar solvent, reduces the overall polarity of the solvent system, thereby influencing the crystallization kinetics of MOFs. ISO plays a crucial role in regulating crystal growth, leading to the formation of BiBTC with a porous structure or smaller crystal sizes. By adjusting the DMF/ISO ratio (5:1, 3:3, 0:6), BiBTC samples with varying crystal sizes, porosity, and surface areas can be obtained, enhancing their photocatalytic performance. This tailored synthesis approach not only improves adsorption, storage, and gas-sensing applications but also contributes to the development of more sustainable and eco-friendly materials.

The structure of BiBTC-ISO_x (x = 1, 3, 6) was determined using X-ray diffraction (XRD). The XRD patterns for BiBTC-ISO_x (x = 1, 3, 6) exhibited peaks at 2θ angles of 8.08°, 10.16°, 38.38°, 44.62°, 65.02°, and 75.1° (Figure 1). These results are consistent with those of previous studies. Notably, the peaks at approximately 8.08° and 10.16° correspond to the (240) and (111) crystal planes of CAU-17 (CCDC number: 1426169), respectively [24,31]. With increasing the ISO solvent portion lead to increasing the peak at 10.16°. The presence of these peaks indicated that the BiBTC-ISO_x compounds

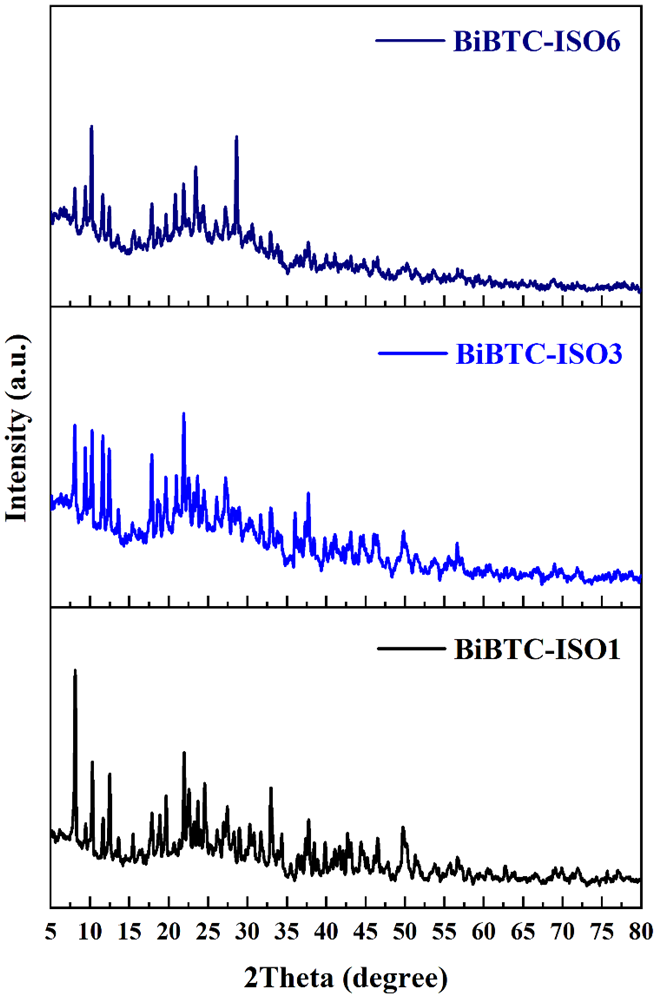

Figure 1. XRD results for BiBTC-ISOx (x = 1, 3, 6)

possessed a crystalline structure similar to that of CAU-17. The intensity and sharpness of the peaks indicated a high degree of crystallinity in the samples. Furthermore, the consistency of the XRD patterns across different x values (1, 3, and 6) implies that the fundamental crystal structure is maintained despite the variations in the ISO content.

FT-IR analysis of the synthesized BiBTC-ISOx (x = 1, 3, 6) catalysts (Figure 2) confirmed successful bonding between the ligand and the Bi^{3+} complex. The absence of the 1721 cm^{-1} (C=O bond) peak and 950 – 890 cm^{-1} (δO–H) peak from the H_3BTC raw material indicates that the (COOH) group bonded with Bi^{3+} [32]. The Bi-BTC material produced with DMF/ISO solvent mixture shows the peak owing to the O–H deformation is located at 3550 cm^{-1}, while ether groups with C–O–C stretch appear at 2790-2813 cm^{-1}. The FT-IR also indicated the peaks at 1437 cm^{-1} (asymmetric stretching of COO) and 1363 cm^{-1} (symmetric stretching of COO). The observed shifts and intensity reductions in the MOF bands indicate the coordination of BTC ligands with Bi^{3+} ions. Additionally, the MOF spectra revealed the appearance of new peaks at a lower wavenumber (~534 cm^{-1}), corresponding to the stretching vibrations of Bi–O bonds [33]. These results suggest the effective functionalization of Bi-BTC with the ligand, as revealed by FTIR analysis.

The optical absorption properties of BiBTC-ISOx (x = 1, 3, and 6) were measured using UV-Vis diffuse reflectance spectroscopy (UV-VIS DRS). The absorption edge of the BiBTC-ISOx catalyst appeared between 343 and 380 nm (Figure 3a). A high absorption intensity was observed in the UV region (below 343 nm), which significantly decreased in the visible region (above 343 nm), indicating a predominant UV absorption. The band gaps of the samples were estimated from the UV-vis absorption data using Equation (2):

$$ahv = A(hv - E_g)^{\eta} \quad (2)$$

where a represents the optical absorption coefficient relative to the optical absorption properties of the semiconductor materials, A is a constant, and h, v, E_g are Planck's constant, light frequency, and bandgap of the semiconductors, respectively.

The bandgaps (E_g) of BiBTC-ISOx (x = 1, 3, and 6) were calculated to be approximately 3.28, 3,6, and 3.68 eV, respectively. This absorption behavior suggests that the BiBTC-ISO catalyst can absorb UV light, which is advantageous for photocatalytic applications (Figure 3b). The variation in the bandgaps across different BiBTC-ISO compositions indicates that the electronic structure of the material can be tuned by adjusting the ratio of its components. This tunability could enable the optimization of the catalyst properties for specific applications or reaction conditions.

Figure 4 presents the results of N_2 adsorption/desorption analyses conducted for

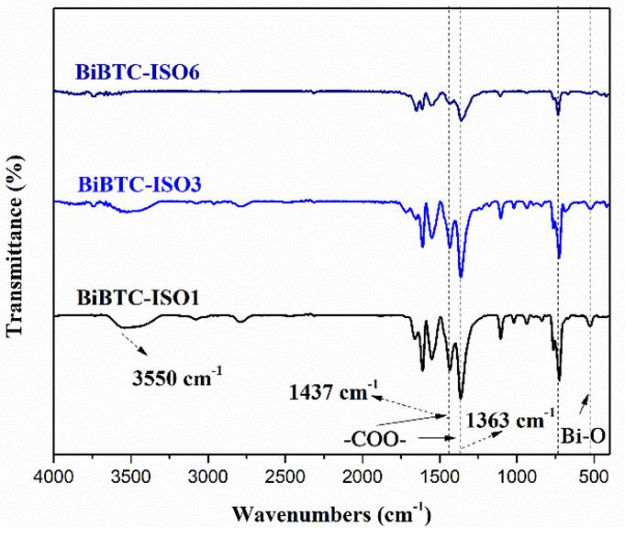

Figure 2. FT-IR spectra of BiBTC-ISOx (x = 1, 3, and 6)

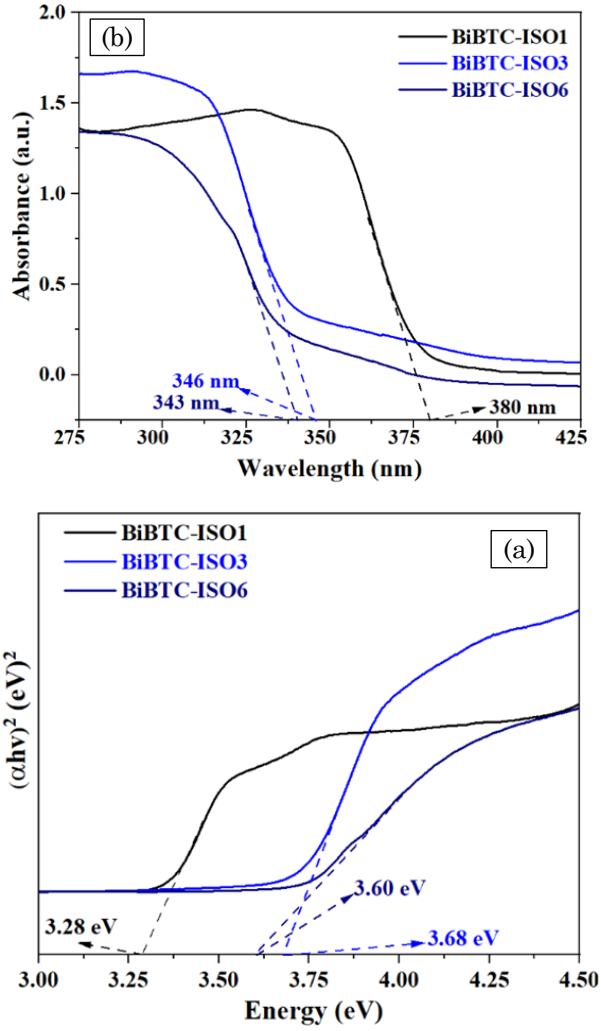

Figure 3. a) UV-Vis spectra and b) the Tauc plots of the as-synthesized sample

BiBTC-ISO1, BiBTC-ISO3, and BiBTC-ISO6. The maximum total surface area and pore size of BiBTC-ISO6 are 24.968 m^2/g and 2.030 nm, respectively. The BiBTC-ISO adsorption-desorption isotherms demonstrate the presence of a micro/mesoporous structure, as evidenced by the isothermal curves exhibiting a characteristic type IV adsorption isotherm with an H4-type hysteresis loop. This hysteresis loop configuration indicates a mesoporous structure [34], which may facilitate the rapid diffusion of RhB into the pores, potentially resulting in enhanced photocatalytic activity. The pore size distribution analysis further supports the presence of micropores and mesopores in the BiBTC-ISO samples. The hierarchical porous structure of these materials can be attributed to the incorporation of ISO during the synthesis. This unique structural feature may contribute to improved mass transfer and increased accessibility of active sites, potentially enhancing the overall photocatalytic performance of the BiBTC-ISO materials.

The morphology of the BiBTC-ISO_x (x = 1, 3, 6) samples was analyzed using scanning electron microscopy (SEM). Figure 5 shows that BiBTC-ISO_x exhibits a rectangular rod-like structure that is evenly distributed and stacked. The length of these rod-like structures ranged from approximately 2 to 5 µm, with a width of 0.5 to 1 µm. As the ISO content was increased, the rods became more elongated and less aggregated. This morphological evolution suggests that the solvent composition plays a crucial role in controlling the crystal growth and assembly of the BiBTC-ISO structures. The EDS showed that the weight percentage of Bi was 63.78% (Figure 5d).

3.2 Photodegradation Activity

The photocatalytic activity of BiBTC-ISOx (x = 1, 3, 6) was evaluated by the decomposition of RhB under visible light irradiation. Figure 6a shows the effect of the DMF/ISO ratio on the ability of BiBTC-ISOx (x = 1, 3, and 6) to decompose RhB. After 45 min of stirring in the

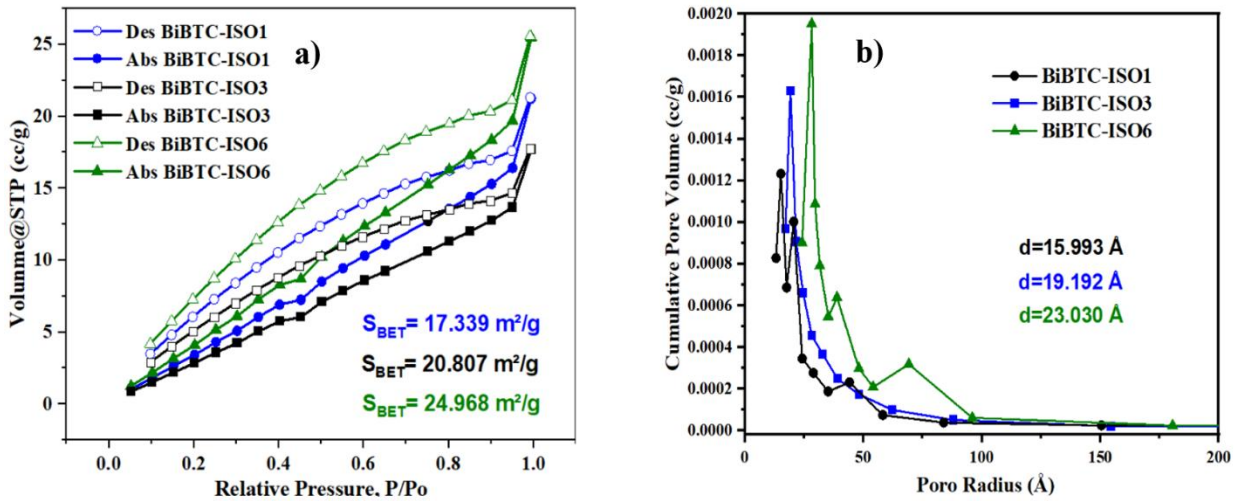

Figure 4. a) Nitrogen adsorption–desorption isotherms, and b) pore size distribution of BiBTC-ISOx (x = 1, 3, and 6).

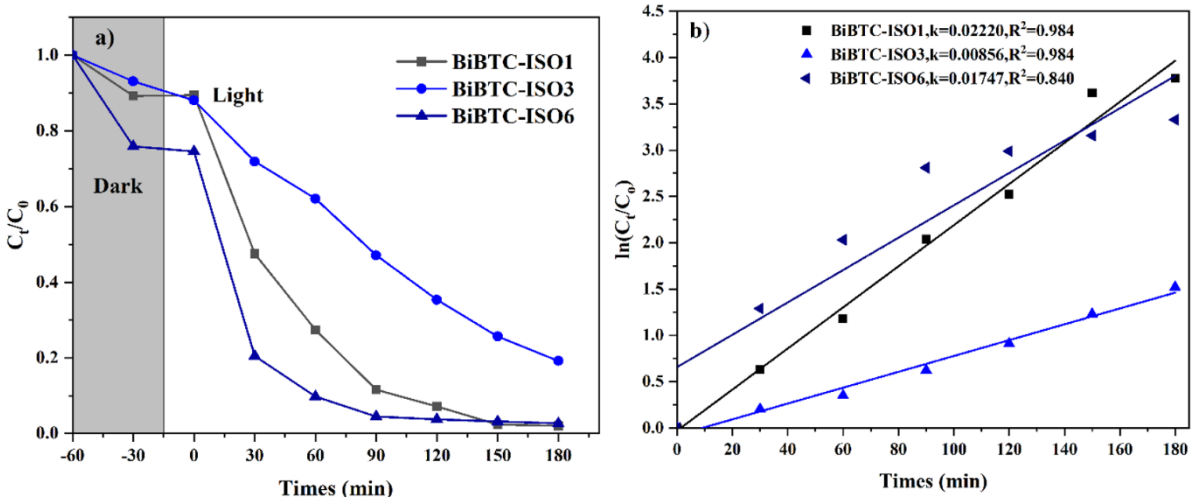

Figure 6. Effect of a) DMF/ISO ratio, b) -ln(C/C_0) graph versus reaction time. Conditions: [Catalyst]=10 mg, [RhB] =15 $mg.L^{-1}$, V= 50 mL, pH=7, light source: white LED (4 × 10 W).

dark, adsorption equilibrium was achieved between the catalyst surface and the RhB molecules. In the presence of the catalyst, the organic content rapidly decreased under visible LED irradiation, indicating that RhB was photocatalytically degraded. This assessment was conducted based on the uptake capacity of RhB and the UV–vis absorption spectral analysis. The RhB uptake capacity of the BiBTC-ISO catalysts followed the order: BiBTC-ISO6 > BiBTC-ISO1 > BiBTC-ISO3. BiBTC-ISO6 exhibited the highest RhB uptake capacity (24.968 mg/g), which was significantly higher than those of the other BiBTC-ISO catalysts. These findings suggest that, among all the BiBTC-ISO catalysts investigated, BiBTC-ISO1 was the most active for RhB degradation. The RhB photodegradation reaction rates were obtained using a pseudo-first-order kinetic model, and the results are shown in Figure 6b. Accordingly, the photodegradation rates decreased in the following order: BiBTC-ISO6 (0.02220 min^{-1}) > BiBTC-ISO1 (0.01747 min^{-1}) > BiBTC-ISO3 (0.00856 min^{-1}), which is consistent with the aforementioned analytical results.

Figure 7a illustrates the influence of catalytic mass on the photocatalytic efficiency of the material. The photocatalytic efficiency increases proportionally with the mass of the material. Under illumination, a catalytic mass of 0.03 g

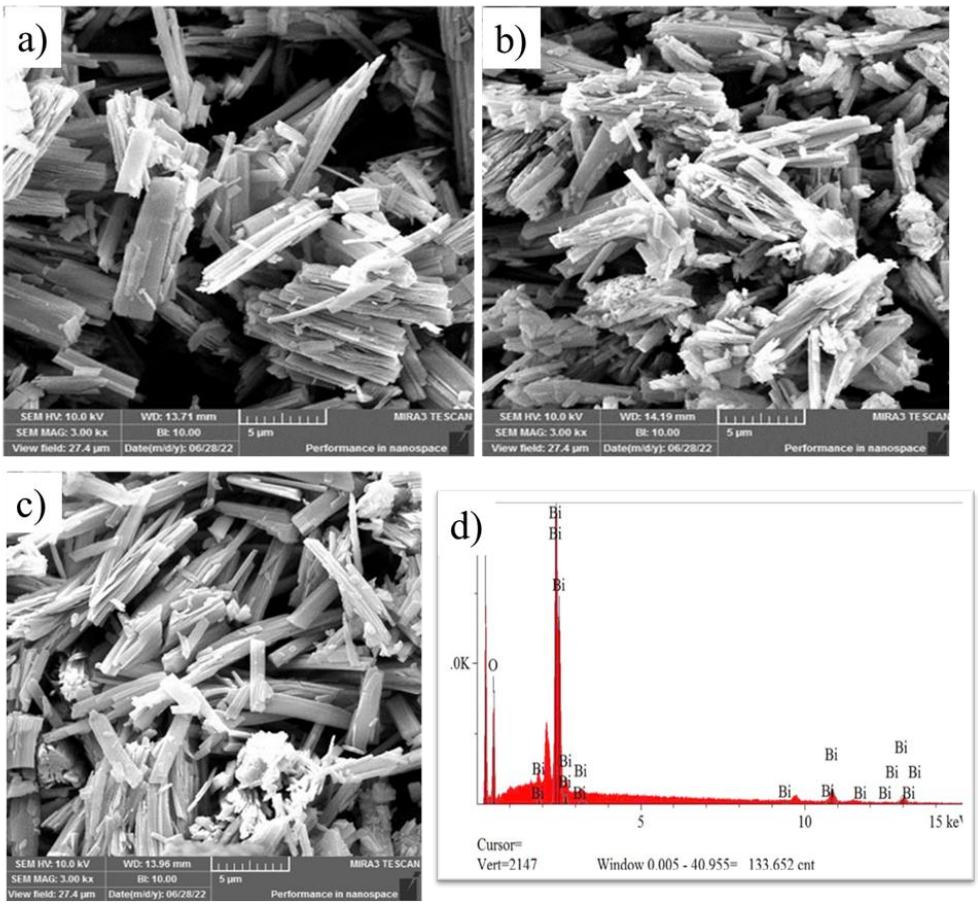

Figure 5. SEM images of a) BiBTC-ISO1, b) BiBTC-ISO3, c) BiBTC-ISO6 and d) EDS of BiBTC-ISO6

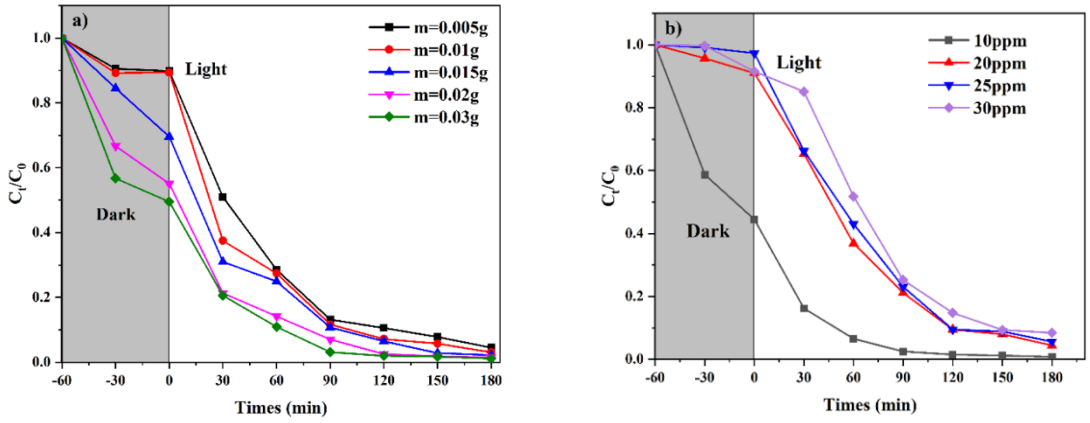

Figure 7. Effect of a) Material mass and b) the RhB concentration on RhB color decomposition. Conditions: [Catalyst]=10 mg, V= 50 mL, pH=7, light source: white LED (40 W).

yielded in the highest RhB removal efficiency, achieving a catalytic efficiency of 98.9% after 180 min of exposure to light. Figure 7b shows that the photocatalytic performance of the material was further investigated at RhB concentrations ranging from 10 to 30 ppm. The photocatalytic performance decreased with increasing RhB concentration. This phenomenon can be attributed to the saturation of the limited active sites on the catalyst surface at higher RhB concentrations, which subsequently affected the efficiency. The optimal RhB concentration was determined to be 10 ppm, which resulted in 99.2% removal (k=0.02238 min^{-1}) after 180 min.

Figure 8a demonstrates that an increase in pH leads to a decrease in photocatalytic efficiency. At pH of 3, RhB removal reached 98.6 % after 180 min of illumination, which can be attributed to the higher number of active sites on the catalyst surface, thereby enhancing RhB adsorption and degradation. The observed decrease in performance at higher RhB concentrations may be a consequence of active site saturation, thus limiting the degradation efficiency. The pH dependence suggests optimal efficiency under neutral or slightly acidic conditions, which can be explained by the catalyst surface charge and RhB stability. Figure 8b indicates that the isoelectric point (IEP) of BiBTC-ISO6 is 3.08, signifying that the catalyst surface exhibits a positive charge below pH of 3.08 and a negative charge above this value. This information is crucial for elucidating the effects of BiBTC-ISO6 on the RhB degradation efficiency. Under acidic conditions, the positively charged catalyst surface enhances electrostatic interactions with negatively charged dye molecules, thereby improving dye removal efficiency.

Transient photocurrent response tests were performed to evaluate the electron-hole separation abilities of BiBTC-ISOx (x = 1, 3, and 6). As shown in Figure 9, BiBTC-ISO6 exhibits a less pronounced photocurrent response than BiBTC-ISO1 and BiBTC-ISO3. The enhanced light absorption and BET surface area increased the photocurrent intensity, indicating better electron-hole separation. Among the samples, BiBTC-ISO6 showed the highest photocurrent intensity, suggesting that it BiBTC-ISO6 generated the most electrons under light irradiation, leading to superior photogenerated carrier separation. The electrochemical impedance spectroscopy (EIS) Nyquist plots in Figure 9 confirms the improved charge-transfer properties. The smallest arc radius in the Nyquist plot was observed for BiBTC-ISOx, followed by

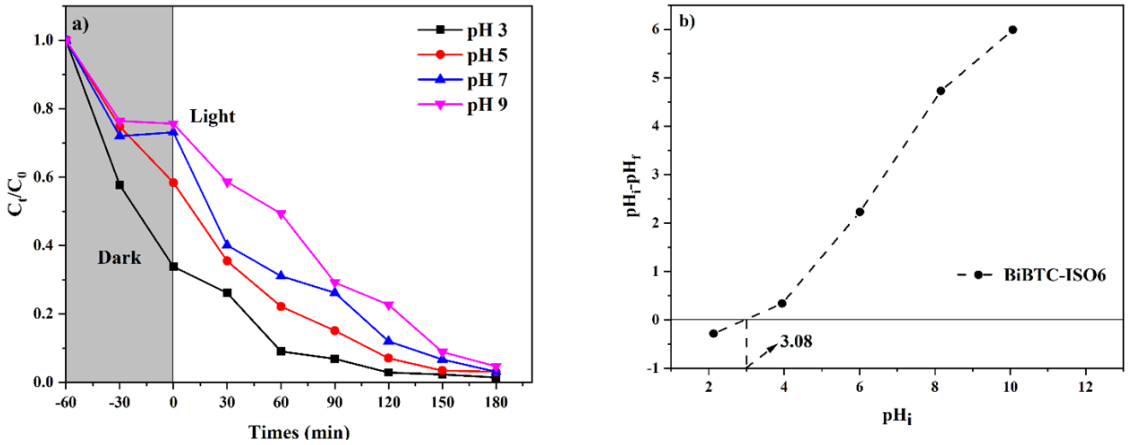

Figure 8. Effect of: a) pH on RhB color decomposition, and b) the isoelectric point (IEP) of BiBTC-ISO6. Conditions: [Catalyst]=10 mg, [RhB] = 15 mg.L^{-1}, V= 50 mL, light source: white LED (4 × 10 W).

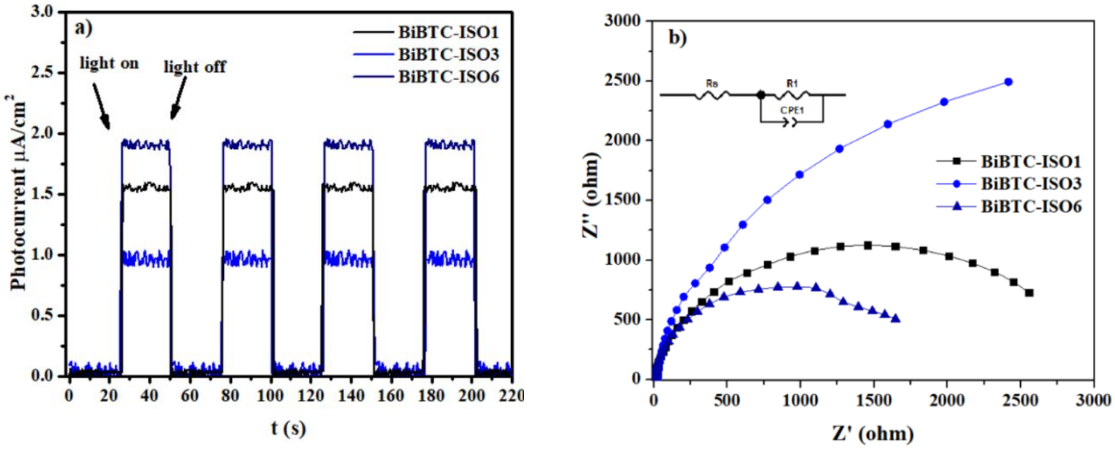

Figure 9. a) Photocurrent and b) EIS plot of BiBTC-ISOx (x = 1, 3, and 6).

BiBTC-ISO1 and BiBTC-ISO3, indicating that BiBTC-ISO6 had the lowest charge transfer resistance. Reduced charge transfer resistance is vital for enhancing photocatalytic activity by promoting efficient charge separation and reducing electron-hole recombination.

3.3 Photocatalytic Mechanism

The photocatalytic mechanism of BiBTC-ISO6 was elucidated by the addition of radical trapping agents to the photocatalytic reaction (Figure 10). Free radical traps for hydroxyl radicals (·OH), electrons (e^-), holes (h^+), and superoxide radicals ($O_2^{\cdot-}$) were employed using tert-Butyl alcohol (TBA), $K_2Cr_2O_7$, $Na_2C_2O_4$, and *p*-benzoquinone (BQ), respectively. The addition of BQ significantly reduced the photocatalytic efficiency, indicating that superoxide radicals ($O_2^{\cdot-}$) played a crucial role in RhB degradation. The slight inhibition was observed with TBA and $Na_2C_2O_4$ suggests that hydroxyl radicals (·OH) are the secondary contributors that interact with $O_2^{\cdot}$ to facilitate dye degradation.

BiBTC-ISO6 exhibits a CB potential of −0.4 eV vs NHE and a VB potential of +3.27 eV. Upon visible-light irradiation, the hole-electron pairs of BiBTC-ISO6 were excited. The photogenerated electrons of BiBTC-ISO6 are more negative than those of $O_2/{}^{\cdot}O_2$ (-0.33 V vs NHE), making electrons susceptible to capture by O_2 to produce $O_2^{\cdot-}$. The photogenerated hole of BiBTC-ISO6 possess a greater positive EVB (3.18 V vs NHE) than $H_2O/{}^{\cdot}OH$ (2.14 V vs NHE), enabling the oxidation of H_2O to ·OH. Consequently, RhB (or $RhB^{\cdot+}$) is effectively degraded by $O_2^{\cdot-}$, ·OH, and h^+.

$$BiBTC\text{-}ISO6 + h\nu \rightarrow BiBTC\text{-}ISO6\ (h^+ + e^-) \quad (3)$$

$$BiBTC\text{-}ISO6\ (e^-) + O_2 \rightarrow O_2^{\cdot-} \quad (4)$$

$$RhB + h\nu \rightarrow RhB^* \quad (5)$$

$$BiBTC\text{-}ISO6\ (h^+) + H_2O \rightarrow {}^{\cdot}OH + H^+ \quad (6)$$

$$O_2^{\cdot-}(\text{or/and } h^+ \text{ and } e^-) + RhB^* \rightarrow \text{Oxidation products} \quad (7)$$

3.4 Reusability and Stability of the Photocatalyst

The durability and reusability of the BiBTC-ISO6 catalyst in photochemical reactions were evaluated. The catalyst exhibited the capacity to consistently degrade RhB dye under visible-light conditions, successfully completing three cycles of catalytic decomposition. Figure 11 shows the ability of BiBTC-ISO6 to degrade RhB pigments. After three consecutive applications, the efficiency of the catalyst for the decomposition of RhB remained largely unaltered. These results suggest that BiBTC-ISO6 possesses exceptional stability and can be effectively reused in catalytic reactions for organic dye degradation.

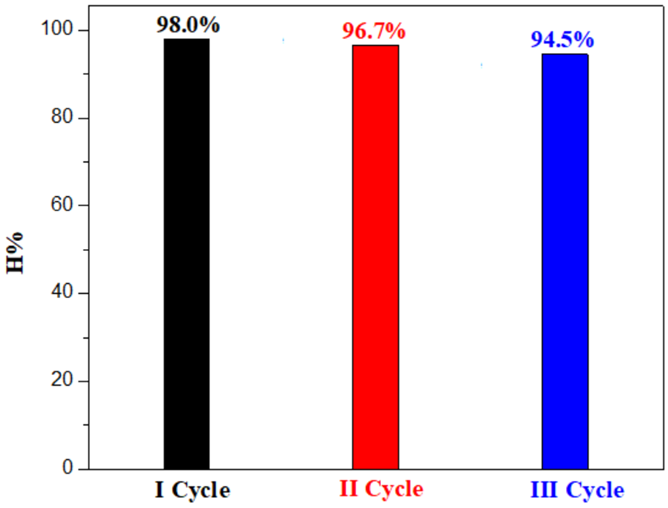

Figure 11. RhB color decomposition ability of BiBTC-ISO6 after three cycles. Conditions: [catalyst]=10 mg, [RhB]=15 mg.L^{-1}, V= 50 mL, and pH=7. Light source: White light LED (4 × 10 W)

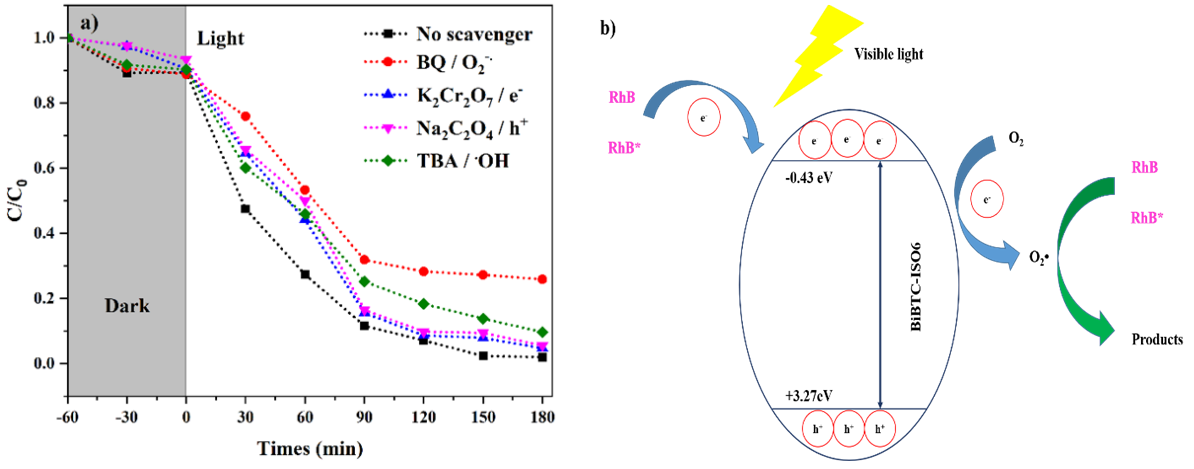

Figure 10. a) Effects of different scavengers on the degradation of RhB and b) Photodegradation mechanism of RhB over BiBTC-ISO6. Conditions: [catalyst] = 10 mg, [RhB] = 15 mg.L^{-1}, and V = 50 mL. Light source: White LED (4 × 10 W), [Scavenger] = 2 × 10^{-4} mg.L^{-1}.

4. Conclusions

This study successfully synthesized and characterized BiBTC-ISO_x (x = 1, 3, 6) catalysts under different DMF/ISO solvent ratios. The findings revealed that the solvent composition significantly influenced the morphology and photocatalytic properties of the catalysts for Rhodamine B (RhB) degradation under visible light irradiation. Photocatalytic performance evaluations under various conditions demonstrated that BiBTC-ISO_6 exhibited the highest activity, achieving 98% RhB removal at pH of 3 after 180 min of illumination. The photocatalytic mechanism was further investigated through radical trapping experiments, which confirmed that superoxide radicals ($O_2^{\cdot-}$) played a dominant role in the degradation process. Additionally, BiBTC-ISO6 exhibited remarkable stability and reusability, maintaining its photocatalytic efficiency over multiple RhB degradation cycles. These results suggest that BiBTC-ISO, particularly BiBTC-ISO_6, holds significant potential as an efficient and sustainable photocatalyst for environmental remediation, particularly in treating organic dye pollutants in wastewater.

Acknowledgment

The authors would like to thank the Industrial University of Ho Chi Minh University for facility support.

CRediT Author Statement

Authors Contributions: Methodology and formal analysis (Pham Bui Bao Long); Supervision and Investigation (Van Cuong Nguyen); Data curation and Investigation (Hoang Ai Le Pham); Writing - Review and Editing (Qui Thanh Hoai Ta); Conceptualization, writing the original draft, and methodology (Huu Phuc Dang). All authors have read and agreed to the published version of the manuscript.

References

[1] Nguyen, S.N., Truong, T.K., You, S.J., Wang, Y.F., Cao, T.M., Pham, V. Van (2019). Investigation on Photocatalytic Removal of NO under Visible Light over Cr-Doped ZnO Nanoparticles. *ACS Omega*, 4(7), 12853–12859. DOI: 10.1021/acsomega.9b01628.

[2] Van Pham, V., La, H.P.P., Le, T.Q., Nguyen, P.H., Van Le, T., Cao, T.M. (2023). Fe2O3/diatomite materials as efficient photo-Fenton catalysts for ciprofloxacin removal. *Environmental Science and Pollution Research*, 30(12), 33686–33694. DOI: 10.1007/s11356-022-24522-3.

[3] Chen, X., Zhu, L., Ma, Z., Wang, M., Zhao, R., Zou, Y., Fan, Y. (2022). Ag Nanoparticles Decorated ZnO Nanorods as Multifunctional SERS Substrates for Ultrasensitive Detection and Catalytic Degradation of Rhodamine B. *Nanomaterials*, 12(14) DOI: 10.3390/nano12142394.

[4] Abdel-Aziz, R., Ahmed, M.A., Abdel-Messih, M.F. (2020). A novel UV and visible light driven photocatalyst AgIO4/ZnO nanoparticles with highly enhanced photocatalytic performance for removal of rhodamine B and indigo carmine dyes. *Journal of Photochemistry and Photobiology A: Chemistry*, 389, 112245. DOI: 10.1016/j.jphotochem.2019.112245.

[5] Kadem, A.J., Tan, Z.M., Suntharam, N.M., Pung, S.Y., Ramakrishnan, S. (2023). Synthesis of CuO, ZnO and SnO2 Coupled TiO2 Photocatalyst Particles for Enhanced Photodegradation of Rhodamine B Dye. *Bulletin of Chemical Reaction Engineering & Catalysis*, 18(3), 506-520. DOI: 10.9767/bcrec.19532.

[6] Pham, V. Van, Truong, T.K., Hai, L.V., La, H.P.P., Nguyen, H.T., Lam, V.Q., Tong, H.D., Nguyen, T.Q., Sabbah, A., Chen, K.-H., You, S.-J., Cao, T.M. (2022). S-Scheme α-Fe2O3/g-C3N4 Nanocomposites as Heterojunction Photocatalysts for Antibiotic Degradation. *ACS Applied Nano Materials*, 5(3), 4506–4514. DOI: 10.1021/acsanm.2c00741.

[7] Vo, N.T.T., You, S.-J., Pham, M.-T., Pham, V. Van (2023). A green synthesis approach of p-n CuO/ZnO junctions for multifunctional photocatalysis towards the degradation of contaminants. *Environmental Technology & Innovation*, 32, 103285. DOI: 10.1016/j.eti.2023.103285.

[8] Gao, X., Huang, G., Gao, H., Pan, C., Wang, H., Yan, J., Liu, Y., Qiu, H., Ma, N., Gao, J. (2016). Facile fabrication of Bi2S3/SnS2 heterojunction photocatalysts with efficient photocatalytic activity under visible light. *Journal of Alloys and Compounds*, 674, 98–108. DOI: 10.1016/j.jallcom.2016.03.031.

[9] Pham, H.A. Le, Vo, T.K., Nguyen, D.T., Huynh, H.K., Pham, Q.T.S., Nguyen, V.C. (2022). Facile synthesis of bismuth terephthalate metal–organic frameworks and their visible-light-driven photocatalytic activities toward Rhodamine B dye. *Green Chemistry Letters and Reviews*, 15(3), 572–581. DOI: 10.1080/17518253.2022.2117998.

[10] Sellam, M., Azizi, S., Bouras, D., Fellah, M., Obrosov, A., El-Hiti, G.A. (2024). Degradation of rhodamine B dye under visible and solar light on zinc oxide and nickel-doped zinc oxide thin films. *Optical Materials*, 151, 115316. DOI: 10.1016/j.optmat.2024.115316.

[11] Chen, D., Cheng, Y., Zhou, N., Chen, P., Wang, Y., Li, K., Huo, S., Cheng, P., Peng, P., Zhang, R., Wang, L., Liu, H., Liu, Y., Ruan, R. (2020). Photocatalytic degradation of organic pollutants using TiO2-based photocatalysts: A review. *Journal of Cleaner Production*, 268, 121725. DOI: 10.1016/j.jclepro.2020.121725.

[12] Wang, Q., Gao, Q., Al-Enizi, A.M., Nafady, A., Ma, S. (2020). Recent advances in MOF-based photocatalysis: Environmental remediation under visible light. *Inorg. Chem. Front.* 7, 300–339. DOI: .....?

[13] Nguyen, T.H.M., Nguyen, V.C., Nguyen, T.H.A. (2025). Photo-reduced synthesis of a Z-scheme Ag@Fe3O4/g-C3N4 composite for photoreduction of 4-nitrophenol and photocatalytic activity. *Brazilian Journal of Chemical Engineering*. DOI: 10.1007/s43153-025-00536-5

[14] Abdi, J., Banisharif, F., Khataee, A. (2021). Amine-functionalized Zr-MOF/CNTs nanocomposite as an efficient and reusable photocatalyst for removing organic contaminants. *Journal of Molecular Liquids*, 334, 116129. DOI: 10.1016/j.molliq.2021.116129.

[15] Yu, F., Jin, M., Zhang, Y., Lei, C., Zhou, L., Zhu, H., Yu, B. (2022). Visible-Light-Driven Zr-MOF/BiOBr Heterojunction for the Efficient Synchronous Removal of Hexavalent Chromium and Rhodamine B from Wastewater. *ACS Omega*, 7(29), 25066–25077. DOI: 10.1021/acsomega.2c01298.

[16] Qin, J., Pei, Y., Zheng, Y., Ye, D., Hu, Y. (2023). Fe-MOF derivative photocatalyst with advanced oxygen reduction capacity for indoor pollutants removal. *Applied Catalysis B: Environmental*, 325, 122346. DOI: 10.1016/j.apcatb.2022.122346.

[17] Zaamouchi, I., Kaci, M.M., Zidane, Y., Belaid, S., Bouacida, S., Benmerad, B. (2024). The impressive photocatalytic performance of Zn-MOF as a novel photocatalyst for the effective purification of dyes under solar exposure. *Journal of Molecular Structure*, 1299, 137070. DOI: 10.1016/j.molstruc.2023.137070.

[18] Wang, Q.-X., Li, G. (2021). Bi(iii) MOFs: syntheses, structures and applications. *Inorganic Chemistry Frontiers*, 8(3), 572–589. DOI: 10.1039/D0QI01055C.

[19] Gao, Y., Yi, X.-H., Wang, C.-C., Wang, F., Wang, P. (2023). Effective Cr(VI) reduction over high throughput Bi-BDC MOF photocatalyst. *Materials Research Bulletin*, 158, 112072. DOI: 10.1016/j.materresbull.2022.112072.

[20] Pham, H.A. Le, Abd, A.A., Nguyen, T.H.A., Le, N.B.T., Nguyen, T.D., Nguyen, V.C., Othman, M.R. (2023). Optimization of photocatalytic degradation performance of organic dye using highly efficient bismuth MOFs: Preparation and parametric analysis. *Chemical Engineering Research and Design*, 198, 196–207. DOI: 10.1016/j.cherd.2023.08.040.

[21] Nguyen, V.H., Nguyen, T.D., Van Nguyen, T. (2020). Microwave-Assisted Solvothermal Synthesis and Photocatalytic Activity of Bismuth(III) Based Metal–Organic Framework. *Topics in Catalysis*, 63(11–14), 1109–1120. DOI: 10.1007/s11244-020-01271-6.

[22] Nguyen, V.H., Pham, A.L.H., Nguyen, V.H., Lee, T., Nguyen, T.D. (2022). Facile synthesis of bismuth(III) based metal-organic framework with difference ligands using microwave irradiation method. *Chemical Engineering Research and Design*, 177(Iii), 321–330. DOI: 10.1016/j.cherd.2021.10.043.

[23] Ye, F., Wei, Z.X., Song, J.F., Wu, X.H., Yue, P. (2017). Synthesis, Characterization, and Photocatalytic Properties of Bismuth (III)-benzene-1,3,5-tricarboxylate. *Zeitschrift fur Anorganische und Allgemeine Chemie*, 643(10), 669–674. DOI: 10.1002/zaac.201700096.

[24] Dong, S., Wang, L., Lou, W., Shi, Y., Cao, Z., Zhang, Y., Sun, J. (2022). Bi-MOFs with two different morphologies promoting degradation of organic dye under simultaneous photo-irradiation and ultrasound vibration treatment. *Ultrasonics Sonochemistry*, 91, 106223. DOI: 10.1016/j.ultsonch.2022.106223.

[25] Gao, Y., Yi, X.-H., Wang, C.-C., Wang, F., Wang, P. (2023). Effective Cr(VI) reduction over high throughput Bi-BDC MOF photocatalyst. *Materials Research Bulletin*, 158, 112072. DOI: 10.1016/j.materresbull.2022.112072.

[26] Zhang, B., Xu, H., Wang, M., Su, L., Zhang, S., Zhang, Y., Wang, Q. (2022). Bismuth (III)-based metal-organic framework for tetracycline removal via adsorption and visible light catalysis processes. *Journal of Environmental Chemical Engineering*, 10(5), 108469. DOI: 10.1016/j.jece.2022.108469.

[27] Łuczak, J., Kroczewska, M., Baluk, M., Sowik, J., Mazierski, P., Zaleska-Medynska, A. (2023). Morphology control through the synthesis of metal-organic frameworks. *Advances in Colloid and Interface Science*, 314, 102864. DOI: https://doi.org/10.1016/j.cis.2023.102864.

[28] Hwang, J., Yan, R., Oschatz, M., Schmidt, B.V.K.J. (2018). Solvent mediated morphology control of zinc MOFs as carbon templates for application in supercapacitors. *Journal of Materials Chemistry A*, 6(46), 23521–23530. DOI: 10.1039/C8TA07700B.

[29] Zhang, B., Zhang, J., Liu, C., Sang, X., Peng, L., Ma, X., Wu, T., Han, B., Yang, G. (2015). Solvent determines the formation and properties of metal–organic frameworks. *RSC Advances*, 5(47), 37691–37696. DOI: 10.1039/C5RA02440D.

[30] Akhundzadeh Tezerjani, A., Halladj, R., Askari, S. (2021). Different view of solvent effect on the synthesis methods of zeolitic imidazolate framework-8 to tuning the crystal structure and properties. *RSC Advances*, 11(32), 19914–19923. DOI: 10.1039/D1RA02856A.

[31] Pham, H.A. Le, Nguyen, V.H., Lee, T., Nguyen, V.C., Nguyen, T.D. (2024). Construction of BiOCl/bismuth-based halide perovskite heterojunctions derived from the metal-organic framework CAU-17 for effective photocatalytic degradation. *Chemosphere*, 357, 142114. DOI: 10.1016/j.chemosphere.2024.142114.

[32] Pham, H.A. Le, Nguyen, D.T., Nguyen, V.C., Ky Vo, T. (2024). Integrating Bi-containing metal–organic frameworks for enhancing their LED visible-light-driven photocatalytic activities towards Rhodamine dye. *Inorganic Chemistry Communications*, 159 DOI: 10.1016/j.inoche.2023.111822.

[33] Liu, X., Su, Y., Zhao, Q., Du, C., Liu, Z. (2016). Constructing Bi24O31Cl10 / BiOCl heterojunction via a simple thermal annealing route for achieving enhanced photocatalytic activity and selectivity. *Scientific Reports*, 6(1), 28689. DOI: 10.1038/srep28689.

[34] Chai, W., Yin, W., Wang, K., Ye, W., Tang, B., Rui, Y. (2019). Carbon-coated bismuth nanospheres derived from Bi-BTC as a promising anode material for lithium storage. *Electrochimica Acta*, 325, 134927. DOI: 10.1016/j.electacta.2019.134927.